Available online at www.sciencedirect.com
SCIENCE DIRECT®
Journal of Computational Physics 190 (2003) 100–117
JOURNAL OF COMPUTATIONAL PHYSICS
www.elsevier.com/locate/jcp

Lattice Boltzmann method and gas-kinetic BGK scheme in the low-Mach number viscous flow simulations

Kun Xu [a,*], Xiaoyi He [b]

[a] Department of Mathematics, Hong Kong University of Science and Technology, Clear Water Bay, Kowloon, Hong Kong
[b] Air Products and Chemicals Inc., Allentown, USA

Received 24 June 2002; received in revised form 23 April 2003; accepted 5 May 2003

Abstract

Both lattice Boltzmann method (LBM) and the gas-kinetic BGK scheme are based on the numerical discretization of the Boltzmann equation with collisional models, such as, the Bhatnagar–Gross–Krook (BGK) model. LBM tracks limited number of particles and the viscous flow behavior emerges automatically from the intrinsic particle stream and collisions process. On the other hand, the gas-kinetic BGK scheme is a finite volume scheme, where the time-dependent gas distribution function with continuous particle velocity space is constructed and used in the evaluation of the numerical fluxes across cell interfaces. Currently, LBM is mainly used for low Mach number, nearly incompressible flow simulation. For the gas-kinetic scheme, the application is focusing on the high speed compressible flows. In this paper, we are going to compare both schemes in the isothermal low-Mach number flow simulations. The methodology for developing both schemes will be clarified through the introduction of operator splitting Boltzmann model and operator averaging Boltzmann model. From the operator splitting Boltzmann model, the error rooted in many kinetic schemes, which are based on the decoupling of particle transport and collision, can be easily understood. As to the test case, we choose to use the 2D cavity flow since it is one of the most extensively studied cases. Detailed simulation results with different Reynolds numbers, as well as the benchmark solutions, are presented.

AMS: 65M06; 65N06; 76P05; 76T05

Keywords: Lattice Boltzmann method; Gas-kinetic method; Isothermal Navier–Stokes equations; Chapman–Enskog expansion; Cavity flow

1. Introduction

Lattice Boltzmann method (LBM) and the gas-kinetic scheme BGK are based on the kinetic equations for solving hydrodynamic systems described by the Navier–Stokes equations. The LBM is fully discrete in

* Corresponding author. Fax: +852-2358-1643.
E-mail addresses: makxu@ust.hk (K. Xu), hex@apci.com (X. He).

0021-9991/$ - see front matter © 2003 Elsevier B.V. All rights reserved.
doi:10.1016/S0021-9991(03)00255-9

time and phase space, which is a simplified version of the continuous Boltzmann equation. Due to the sampling of the particle velocities around zero velocity, LBM is limited to the low-Mach number (nearly incompressible) flow simulation. The introduction of LBM method and its history can be found in [4,11,21,23], and references therein. From the theoretical analysis and numerical evidence, it is commonly recognized that the LBM can faithfully be used to simulate the incompressible Navier-Stokes equations with high accuracy [10]. Recently, many attempts have been tried to extend the LBM to the compressible flow regime [1,9,13,14,22].

The gas-kinetic BGK scheme is a finite volume scheme, which originally targets to simulate compressible flows. The use of the BGK model here is to construct a time-dependent gas distribution function at a cell interface, from which the numerical fluxes are evaluated. For the compressible flow simulations, the gas-kinetic BGK scheme is verified to be a robust and accurate method, see [24] and references therein. It possesses excellent shock capturing ability and high accuracy for the viscous flow simulations, such as the capturing of the Navier–Stokes shock structure and laminar boundary layer. In this paper, for the first time we are going to extend the gas-kinetic BGK scheme to the nearly incompressible isothermal flow simulations. In order to get a clear idea about the similarity and differences between the LBM and the gas-kinetic BGK scheme, the physical basis for both schemes will be analyzed. In an earlier paper, the gas-kinetic BGK scheme is extended to the low-Mach number flow computation [20]. Since the energy equation is still kept there, due to the viscous heating it may not have a clear connection with LBM. In order to have a more fair comparison, the gas-kinetic BGK scheme and the LBM presented here are both for the isothermal Navier–Stokes equations, where the energy equation is absent.

There are many similarities between the LBM and gas-kinetic BGK scheme. Both schemes are inherently time-accurate explicit flow solvers, and a transient process is used to obtain steady state solutions. In this paper, we are going to compare both schemes. As a supplement to the numerical solution in [8], the accuracy of both methods will be tested in the 2D cavity flow simulation, where more detailed velocity profiles along the central lines, as well as benchmark results, will be presented.

2. Lattice Boltzmann method and gas-kinetic scheme

2.1. Bhatnagar–Gross–Krook model for isothermal viscous flow

The gas-kinetic BGK model for the Boltzmann equation is

$$f_t + \boldsymbol{\xi} \cdot \nabla f = (g - f)/\tau, \tag{2.1}$$

where the single particle distribution function $f = f(\mathbf{x}, \boldsymbol{\xi}, t)$ is a time-dependent function of particle coordinate $\mathbf{x}$ and velocity $\boldsymbol{\xi}$, τ is the relaxation time which characterizes typical collision process, and the local Maxwellian equilibrium distribution function defined by

$$g(\rho, \mathbf{u}, \theta) = \rho(2\pi\theta)^{-D/2} \exp[-(\boldsymbol{\xi} - \mathbf{u})^2/2\theta],$$

where D is the dimension of the space $\boldsymbol{\xi}$; ρ, $\mathbf{u}$ and $\theta = kT/m$ are the mass density, macroscopic velocity, and normalized temperature per unit mass, respectively; k, T, and m are the Boltzmann constant, temperature, and molecular mass. Note that the above equilibrium distribution function may be different from the real monatomic, or diatomic gases. For the case $D = 3$, the above g is the equilibrium state for a monatomic gas. However, for $D = 2$, the gas described by the above equilibrium state is limited to move only in a plane without any random motion in the third direction, which does not correspond to any real gas distribution function. Therefore, the above g is only served as a mathematical model for the 2D incompressible flow simulation. As shown in [20], the inclusion of particle random motion in the third direction for a 2D flow

does reduce its accuracy in comparison with the solution of the incompressible equations, especially when the energy equation is included.

Since this paper is about the comparison of the LBM and gas-kinetic BGK method in the 2D case, the following presentation refers to the 2D case only.

The mass density ρ, velocity $\mathbf{u}$, and the temperature θ are the hydrodynamic moments of f and g

$$\rho = \int f \, \mathrm{d}\boldsymbol{\xi} = \int g \, \mathrm{d}\boldsymbol{\xi},$$

$$\rho \mathbf{u} = \int \boldsymbol{\xi} f \, \mathrm{d}\boldsymbol{\xi} = \int \boldsymbol{\xi} g \, \mathrm{d}\boldsymbol{\xi}.$$

For the isothermal equations, θ is a constant. With the Chapman–Enskog expansion, the moments of the above equation lead to the compressible isothermal Navier–Stokes equations

$$\partial_t \rho + \nabla \cdot (\rho \mathbf{u}) = 0,$$

$$\partial_t (\rho \mathbf{u}) + \nabla (\rho \mathbf{u}\mathbf{u} + \rho\theta) = -\nabla \Pi^{(1)},$$

where

$$\Pi^{(1)}_{ij} = \int f^{\mathrm{neq}} \xi_i \xi_j \, \mathrm{d}\xi = -\tau\rho\theta \left(\partial_i u_j + \partial_j u_i - \frac{2}{D} \partial_k u_k \right).$$

In the incompressible limit, i.e., $\rho \simeq$ constant, the kinematic viscosity in the above equation becomes

$$\nu = \tau\theta.$$

The continuous BGK equation (2.1) admits a formal integral solution

$$f(\mathbf{x}, \boldsymbol{\xi}, t + \Delta t) = \frac{1}{\tau} \int_t^{t+\Delta t} g(\mathbf{x}', \boldsymbol{\xi}, t') \mathrm{e}^{-(t+\Delta t - t')/\tau} \, \mathrm{d}t' + \mathrm{e}^{-\Delta t/\tau} f_0(\mathbf{x} - \boldsymbol{\xi}\Delta t, \boldsymbol{\xi}), \tag{2.2}$$

where $f_0(\mathbf{x}, \boldsymbol{\xi})$ is the initial condition at time t, and the particle trajectory is $\mathbf{x} - \mathbf{x}' = \boldsymbol{\xi}(t + \Delta t - t')$. In the above equation, the free transport and collision are coupled at any point in space and time.

2.2. Operator splitting Boltzmann model

In most cases, the free transport and particle collision are separately treated in many kinetic schemes, e.g., DSMC [2] and KFVS [18] methods. These schemes use an operator splitting Boltzmann model. Originally, the lattice Boltzmann method was also considered to be based on the operator splitting Boltzmann model. In the following, from Eq. (2.2), we are going to derive the operator splitting Boltzmann equation. As shown in [6], the assumptions for its derivation are:

(i) The equilibrium state g between the point $(\mathbf{x}, t)$ and $(\mathbf{x} + \boldsymbol{\xi}\Delta t, t + \Delta t)$ is approximated as

$$g(\mathbf{x}', \boldsymbol{\xi}, t') = \left(1 - \frac{t' - t}{\Delta t} \right) g(\mathbf{x}, \boldsymbol{\xi}, t) + \frac{t' - t}{\Delta t} g(\mathbf{x} + \boldsymbol{\xi}\Delta t, \boldsymbol{\xi}, t + \Delta t),$$

where $t' \in [t, t + \Delta t]$.

(ii) $\Delta t/\tau \ll 1$ and

$$\exp(-\Delta t/\tau) \simeq 1 - \Delta t/\tau.$$

Then, the integral solution (2.2) can be approximated as

$$f(\mathbf{x}+\boldsymbol{\xi}\Delta t,\boldsymbol{\xi},t+\Delta t)-f(\mathbf{x},\boldsymbol{\xi},t)=\frac{\Delta t}{\tau}(g(\mathbf{x},\boldsymbol{\xi},t)-f(\mathbf{x},\boldsymbol{\xi},t)). \tag{2.3}$$

The above equation can be considered as a new gas-kinetic model for the Boltzmann equation, where the particle transport and collision are separated in a time interval Δt. Note that the space and phase space are still continuous in the above equation, and time-step Δt is a free parameter, which can be varied under the condition $\Delta t \ll \tau$. In the limiting case, such as $\Delta t \to 0$, the operator splitting kinetic model goes back to the original BGK model. The above operator splitting kinetic model is the underlying governing equations for many kinetic schemes, where the particle motion is composed of the subprocess of transport and collision. As analyzed next, the corresponding macroscopic governing equations for the above equation will be different from the one derived from the BGK model, where the collision and transport are coupled at any point in space and time. But, in terms of macroscopic equations, as shown next, the difference between BGK and the above operator splitting model is mainly coming from the modification of viscosity coefficient.

In the above operator splitting Boltzmann model, the space $\mathbf{x}$ and phase space $\boldsymbol{\xi}$ are continuous, and Δt is a small time increment. Note that there is no lattice concept involved yet. Instead of Eq. (2.1), Eq. (2.3) can be considered as a new governing equation. The corresponding macroscopic equations for Eq. (2.3) can be derived before the construction of any numerical schemes to solve it. With the Taylor expansion,

$$f(\mathbf{x}+\boldsymbol{\xi}\Delta t,\boldsymbol{\xi},t+\Delta t)=\sum_{n=0}^{\infty}\frac{\Delta t^n}{n!}D_t^n f(\mathbf{x},\boldsymbol{\xi},t),$$

where $D_t=(\partial_t+\boldsymbol{\xi}\cdot\nabla)$, substituting the above expansion into Eq. (2.3), and up to $(\Delta t)^2$, the governing equation (2.3) becomes

$$D_t f+\frac{\Delta t}{2}D_t^2 f=-\frac{1}{\tau}(f-g), \tag{2.4}$$

where g is the equilibrium state. When using Eq. (2.4) to study the macroscopic flow behavior with a time and length scales $\mathscr{T}$ and $\mathscr{L}$ with $\tau \ll \mathscr{T}$, the above equation can be written in a dimensionless form

$$D_{\tilde{t}} f+\frac{\epsilon_0}{2}D_{\tilde{t}}^2 f=-\frac{1}{\epsilon}(f-g), \tag{2.5}$$

where $D_{\tilde{t}}=\mathscr{T}D_t$, $\epsilon=\tau/\mathscr{T}$, and $\epsilon_0=\Delta t/\mathscr{T}<\epsilon$. With the expansion of the distribution function

$$f=\sum_{m=0}^{\infty}\epsilon^m f^{(m)}=g+\sum_{m=1}^{\infty}\epsilon^m f^{(m)}=g+f^{\mathrm{neq}},$$

and substituting the above expansion into Eq. (2.5), we have

$$\begin{aligned}
&\epsilon^0 : D_{\tilde{t}} g=-f^{(1)},\\
&\epsilon^1 : D_{\tilde{t}} f^{(1)}+\frac{\epsilon_0}{2\epsilon}D_{\tilde{t}}^2 g=-f^{(2)},\\
&\epsilon^2 : D_{\tilde{t}} f^{(2)}+\frac{\epsilon_0}{2\epsilon}D_{\tilde{t}}^2 f^{(1)}=-f^{(3)},\\
&\vdots
\end{aligned}$$

The compatibility conditions for the above equations are

$$\int \begin{pmatrix} 1 \\ \boldsymbol{\xi} \end{pmatrix} f^{(m)} \, \mathrm{d}\boldsymbol{\xi} = 0 \quad \text{for} \quad m = 1, 2, \ldots.$$

Taking moments $(1, \boldsymbol{\xi})^{\mathrm{T}}$ on the equation with order ϵ^0, we can get the isothermal Euler equations. Taking the moments $(1, \boldsymbol{\xi})^{\mathrm{T}}$ on Eq. (2.5) with order ϵ^1 and using the compatibility condition, the isothermal Navier–Stokes equations can be obtained, where the viscosity coefficient v is

$$v = \tau\left(1 - \frac{\Delta t}{2\tau}\right)\theta = \left(\tau - \frac{\Delta t}{2}\right)\theta. \tag{2.6}$$

Due to the continuous nature of the phase space in Eq. (2.3), the Navier–Stokes equations including the correct energy equation can be also derived from it with the modification of viscosity and heat conduction coefficients. In other words, the model (2.3) can be faithfully applied to the compressible flow simulations. Then, the problem becomes how to numerically solve it. For example, Sun's scheme for compressible flow simulation is one of the methods to solve Eq. (2.3) [22]. Since a small time increment involved in the viscosity coefficient, in order to construct a scheme based on Eq. (2.3) with constant dissipative coefficients, a uniform time increment is required. Also, due to the condition $\tau \gg \Delta t$, with a fixed time increment Δt, the particle collision time has to be set beyond a certain value. For the high Reynolds number flow simulation, where v has a small value, Eq. (2.6) requires $\tau \simeq \Delta t/2$, which may violate the condition to derive the operator splitting model. Therefore, it should be cautious to apply these schemes based on Eq. (2.3) in the high Reynolds number flow simulations. If the additional term related to Δt in v of the macroscopic equations is ignored, theoretically the operator splitting kinetic model becomes only a first-order accurate method for the viscous governing equations. The analysis in [15] basically points out the splitting error in Eq. (2.3) when $\Delta t/2$ is not included in the physical viscosity coefficient.

After having the governing equation (2.3), the main task left is how to use it to design a numerical scheme. Many schemes, such as kinetic flux vector splitting schemes are coming from the above splitting model [18]. The gas-kinetic BGK scheme presented in Section 2.5 is based on Eq. (2.2) directly, where the transport and collision take place continuously in space and time.

2.3. Operator averaging Boltzmann model

Rather than assuming the particle transport in any time-step is free of collision as in the Operator-Splitting-Boltzmann model, we may also assume the particle collision effect in a given time period takes the average value of those at the beginning and end of the period. By doing so, the BGK equation (2.1) becomes

$$f(\mathbf{x} + \boldsymbol{\xi}\Delta t, \boldsymbol{\xi}, t + \Delta t) - f(\mathbf{x}, \boldsymbol{\xi}, t) = -\frac{\Delta t}{2\tau}(f^{\mathrm{neq}}(\mathbf{x} + \boldsymbol{\xi}\Delta t, \boldsymbol{\xi}, t + \Delta t) + f^{\mathrm{neq}}(\mathbf{x}, \boldsymbol{\xi}, t)). \tag{2.7}$$

Unlike in the Operator-Splitting model (see last section), Δt in an Operator-Averaging model is unlimited by τ. With the introduction of

$$\bar{f} = f + \frac{\Delta t}{2\tau} f^{\mathrm{neq}}, \tag{2.8}$$

the governing equation of $\bar{f}$ becomes

$$\bar{f}(\mathbf{x} + \boldsymbol{\xi}\Delta t, \boldsymbol{\xi}, t + \Delta t) - \bar{f}(\mathbf{x}, \boldsymbol{\xi}, t) = -\frac{\Delta t}{\tau + \Delta t/2}(\bar{f}(\mathbf{x}, \boldsymbol{\xi}, t) - g(\mathbf{x}, \boldsymbol{\xi}, t)). \tag{2.9}$$

Eq. (2.9) is very similar to the Operator-Splitting model (2.3) except two important facts. First, the variable in the governing equation is no longer the particle distribution function anymore. Although the new variable, $\bar{f}$, still satisfies the compatible conditions

$$\rho = \int \bar{f}\,\mathrm{d}\boldsymbol{\xi} = \int g\,\mathrm{d}\boldsymbol{\xi},$$

$$\rho\mathbf{u} = \int \boldsymbol{\xi}\bar{f}\,\mathrm{d}\boldsymbol{\xi} = \int \boldsymbol{\xi} g\,\mathrm{d}\boldsymbol{\xi},$$

it is nevertheless different from the real distribution function. This fact can be clearly demonstrated by the inequality:

$$\begin{aligned}\int \boldsymbol{\xi}\boldsymbol{\xi} f\,\mathrm{d}\boldsymbol{\xi} &= \rho\mathbf{u}\mathbf{u} + \tau\rho\theta\left(\partial_i u_j + \partial_j u_i - \frac{2}{D}\partial_k u_k\right) \neq \int \boldsymbol{\xi}\boldsymbol{\xi}\bar{f}\,\mathrm{d}\boldsymbol{\xi} \\ &= \rho\mathbf{u}\mathbf{u} + (\tau + \Delta t/2)\rho\theta\left(\partial_i u_j + \partial_j u_i - \frac{2}{D}\partial_k u_k\right).\end{aligned}$$

Secondly, the denominator on the right-hand side of Eq. (2.9) is $\tau + \Delta t/2$ instead of τ as in Eq. (2.3). Consequently, the Operator-Averaging model, Eq. (2.9) yields a correct kinematic viscosity of $\nu = \tau\theta$ instead of $\nu = (\tau - \Delta t/2)\theta$ as in the Operator-Splitting model. The time-step in the Operator-Averaging model is not restricted by $\Delta t \ll \tau$ and small τ can be used in practice to simulate high Reynolds number flow.

It should be noted Eqs. (2.3) and (2.9) were mathematically identical if we disregarded the physical meanings of the primary variable and the relaxation parameter. This is why Eq. (2.3) has been long considered as the starting point of the lattice Boltzmann method, despite the fact that LBM is proved to be second-order accurate and the representation of the kinematic viscosity is different from the kinetic theory. In the following section, we will formulate a lattice Boltzmann model based on Eq. (2.9). For simplicity, we will drop the bar of $\bar{f}$ in the following texts.

2.4. Lattice Boltzmann method

The lattice Boltzmann method simulates fluid flow by tracking particle distribution function. Since it is almost impossible to accomplish this task in continuous phase space, the LBM only tracks particle distribution along a handful directions. In another word, LBM solves Eq. (2.9) along a set of discrete velocity in momentum space. Clearly, there are unlimited choices for discretization of phase space, but how to do this in the most efficient way is a challenge. By the most efficient way, we mean to use minimum number of discrete velocities to reproduce real physical laws (e.g., the Navier–Stokes equations).

In LBM, the momentum space is discretized in such a way that any moment integration of the distribution function is approximated by quadrature up to a certain degree of accuracy. Interested readers can go to He and Luo's [6] paper for the derivation of D2Q9 model. For the isothermal Navier–Stokes equations, the moments of the distribution function can be properly calculated by the 7-speed or 9-speed quadrature. For the 9-speed quadrature (D2Q9 model), see Fig. 1, the discretized scheme becomes

$$f_\alpha(\mathbf{x} + \mathbf{e}_\alpha\Delta t, t) - f_\alpha(\mathbf{x}, t) = -\frac{\Delta t}{\tau + 0.5\Delta t}[f_\alpha(\mathbf{x}, t) - g],$$

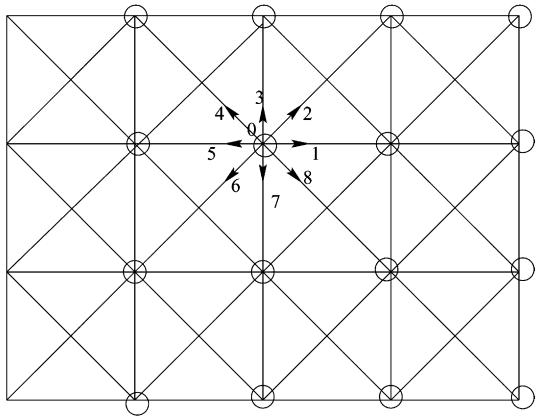

Fig. 1. Schematic description of LBM.

where the equilibrium distribution function is defined as

$$g = w_i\rho\left[1 + 3\frac{\mathbf{e}_i\cdot\mathbf{u}}{c^2} + \frac{9}{2}\frac{(\mathbf{e}_i\cdot\mathbf{u})^2}{c^4} - \frac{3}{2}\frac{(\mathbf{u}\cdot\mathbf{u})}{c^2}\right],$$

where c is related to the grid size Δx and time-step Δt, i.e., $c = \Delta x/\Delta t$. Here w_i is the weight coefficients, which have the following values for D2Q9 models:

$$w_0 = 4/9, \quad w_1 = w_3 = w_5 = w_7 = 1/9, \quad w_2 = w_4 = w_6 = w_8 = 1/36.$$

In order to have the particle moving from one node to another node in a time-step, we have $c = \sqrt{3\theta} = \Delta x/\Delta t$. Therefore, the viscosity coefficient for the D2Q9 model is

$$v = \frac{\tau c^2}{3}. \tag{2.10}$$

Recovering of the energy equation is still a challenging problem in LBM [26]. This problem is not due to the limited number of the particle velocities. In theory, one can always increase the number of discrete velocities if it becomes necessary. Rather, the hurdle comes from the conflict between the synchronization of particle movement in the LBM and the dependence of momentum discretization on local temperature. For high Mach number flow, the momentum discretization should basically depend on local macroscopic velocity. The synchronization of the particle movement means that all particles move from one computational node to another at one time-step. It greatly simplifies the algorithm and facilitates parallel computing. For low-Mach number, isothermal flow, the momentum discretization can be constructed independently of local macroscopic variables and the synchronization of the particle movement can be readily guaranteed. For thermal problem or high Mach number flow, however, this synchronization will inevitably be destroyed and an additional interpolation step has to be introduced to reconstruct the nodal values at next time-step. The thermal LBM scheme constructed this way may recover to the gas-kinetic BGK scheme.

2.5. Gas-kinetic BGK scheme

For a finite volume method, the discretization is accomplished by dividing the flow into a large number of small subdomains in the physical space. Taking the moments $\psi_\alpha = (1, \xi_x, \xi_y)^{\mathrm{T}}$ to the BGK equation (2.1), we have

$$\frac{\mathrm{d}}{\mathrm{d}t}\int_{\Omega}\psi_{\alpha}f\,\mathrm{d}\boldsymbol{\xi}\,\mathrm{d}V+\int_{\partial\Omega}\psi_{\alpha}\boldsymbol{\xi}f\,\mathrm{d}\boldsymbol{\xi}\cdot\mathbf{n}\,\mathrm{d}\sigma=0 \tag{2.11}$$

to each subdomain Ω with boundary $\partial\Omega$, see Fig. 2. Due to the compatibility condition, the collision term has no contribution to the update of the conservative variables inside each cell, but it does effect the fluxes across cell interfaces. In a gas-kinetic BGK scheme, the flux vectors across cell boundaries are calculated based on the gas distribution function. We use Eq. (2.2) to evaluate f at a cell interface, such as the point 0 in Fig. 2. Next, we are going to evaluate the distribution function f at this point.

Denote the location of the interface, such as the point 0 in Fig. 2, as $\mathbf{x}_0=(0,0)$. The initial condition $f_0(\mathbf{x},\boldsymbol{\xi},t=0)$ at the beginning of each time-step around this point $\mathbf{x}_0$ is assumed to be a distribution function truncated to the Navier–Stokes order

$$f_0(\mathbf{x},\boldsymbol{\xi},0)=g(\mathbf{x}_0,\boldsymbol{\xi},0)+f^{(1)}(\mathbf{x}_0,\boldsymbol{\xi},0)+(\mathbf{x}-\mathbf{x}_0)\cdot\nabla g.$$

Here the equilibrium state $g(\mathbf{x}_0,\boldsymbol{\xi},0)$ has the distribution

$$g=\rho_0\left(\frac{\lambda}{\pi}\right)\mathrm{e}^{-\lambda(\boldsymbol{\xi}-\mathbf{u}_0)^2}, \tag{2.12}$$

which can be determined from the macroscopic variables $(\rho_0,\rho_0\mathbf{u}_0)$ there, see Appendix A for the interpolation of the macroscopic variables. For the isothermal NS equations, $\lambda=1/2\theta$ is a constant. With a given Mach number M, λ is determined by

$$\lambda=M^2/(2\mathbf{u}_{\infty}^2).$$

For the BGK model, the non-equilibrium states $f^{(1)}$ is $f^{(1)}=-\tau Dg$, and $D=\partial_t+\boldsymbol{\xi}\cdot\nabla$, which becomes

$$f^{(1)}=-\tau(\partial g/\partial t+\boldsymbol{\xi}\cdot\nabla g).$$

Taking derivative to the equilibrium distribution g gives

$$f^{(1)}=-\tau(a\xi_x+b\xi_y+A)g, \tag{2.13}$$

where $\partial g/\partial x=ag,\ \partial g/\partial y=bg,\ \partial g/\partial t=Ag$ and

$$a=a_1+a_2\xi_x+a_3\xi_y,$$

$$b=b_1+b_2\xi_x+b_3\xi_y,$$

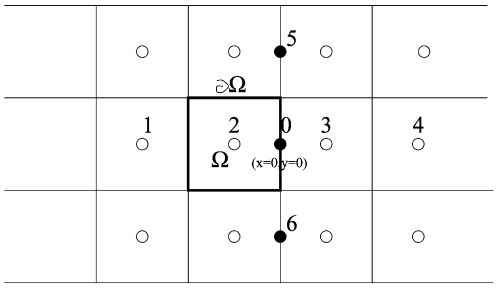

Fig. 2. A finite volume gas-kinetic BGK scheme, where the flow variables at the interface, such as at points 0, 5, and 6, need to be interpolated from the cell averaged values.

$$A = A_1 + A_2\xi_x + A_3\xi_y.$$

The coefficients $a_1, a_2, \ldots, b_3$ can be found from the relation

$$\int\int \begin{pmatrix} 1 \\ \xi_x \\ \xi_y \end{pmatrix} ag\,\mathrm{d}\xi_x\,\mathrm{d}\xi_y = \begin{pmatrix} \partial\rho/\partial x \\ \partial(\rho u)/\partial x \\ \partial(\rho v)/\partial x \end{pmatrix}$$

and

$$\int\int \begin{pmatrix} 1 \\ \xi_x \\ \xi_y \end{pmatrix} bg\,\mathrm{d}\xi_x\,\mathrm{d}\xi_y = \begin{pmatrix} \partial\rho/\partial y \\ \partial(\rho u)/\partial y \\ \partial(\rho v)/\partial y \end{pmatrix}.$$

The interpolation of the macroscopic variables of ρ and $\rho\mathbf{u}$ around point 0 in Fig. 2 is presented in Appendix A. Appendix B gives the method to get these coefficients in a and b from the above equations. After determining a and b, the term A in Eq. (2.13) is obtained from the compatibility condition

$$\int\int \begin{pmatrix} 1 \\ \xi_x \\ \xi_y \end{pmatrix} f^{(1)}\,\mathrm{d}\xi_x\,\mathrm{d}\xi_y = 0,$$

which gives

$$\int\int \begin{pmatrix} 1 \\ \xi_x \\ \xi_y \end{pmatrix} Ag\,\mathrm{d}\xi_x\,\mathrm{d}\xi_y = -\int\int \begin{pmatrix} 1 \\ \xi_x \\ \xi_y \end{pmatrix} (a\xi_x + b\xi_y)g\,\mathrm{d}\xi_x\,\mathrm{d}\xi_y.$$

Since a and b are known, the value of A_1, A_2, and A_3 in A can be obtained using Appendix B again. Therefore, in the 2D case with x, y coordinates, f_0 at time $t = 0$ can be written as

$$f_0(\mathbf{x}, \boldsymbol{\xi}, t) = g\big(1 - \tau(a\xi_x + b\xi_y + A) + ax + by\big). \tag{2.14}$$

Note that for the isothermal incompressible NS equations, the solutions are supposed to be smooth, i.e., no shocks formed, the *kinematic* dissipation through the introduction of discontinuity at a cell interface is not included in the above expression of f_0 [24].

The equilibrium distribution in space and time around point $(\mathbf{x}_0, t = 0)$ can be obtained from the expansion of an equilibrium state

$$g(\mathbf{x}, \boldsymbol{\xi}, t) = g(\mathbf{x}_0, \boldsymbol{\xi}, 0) + (\partial g/\partial x)x + (\partial g/\partial y)y + (\partial g/\partial t)t = g(1 + ax + by + At).$$

Substituting both g and f_0 into the integral solution (2.2), the distribution function at a cell interface becomes

$$f(\mathbf{x}_0, \boldsymbol{\xi}, t) = g(1 - \tau(a\xi_x + b\xi_y + A) + tA), \tag{2.15}$$

from which the fluxes across the cell interface can be evaluated. For example, based on the above f, the flux in the x-direction at point 0 becomes

$$\begin{pmatrix} \mathscr{F}_\rho \\ \mathscr{F}_{\rho\mathbf{u}} \end{pmatrix}_{i+1/2,j} = \int\int \xi_x \begin{pmatrix} 1 \\ \boldsymbol{\xi} \end{pmatrix} f(\mathbf{x}_0, \boldsymbol{\xi}, t)\,\mathrm{d}\xi_x\,\mathrm{d}\xi_y. \tag{2.16}$$

Theoretically, it has been shown that in the smooth region Eq. (2.15) is truly solving the Navier–Stokes equations [16]. Similarly, $\mathscr{G}_{i,j+1/2}$, the fluxes in the y direction at other boundaries can be obtained using

the above process. With both fluxes in the x and y directions, Eq. (2.11) becomes a discretized form for the cell Ω

$$\begin{pmatrix} \rho \\ \rho \mathbf{u} \end{pmatrix}_{\Omega}^{n+1} = \begin{pmatrix} \rho \\ \rho \mathbf{u} \end{pmatrix}_{\Omega}^{n} + \int_0^{\Delta t} \left(\frac{1}{\Delta x} (\mathscr{F}_{i-1/2,j} - \mathscr{F}_{i+1/2,j}) + \frac{1}{\Delta y} (\mathscr{G}_{i,j-1/2} - \mathscr{G}_{i,j+1/2}) \right) \mathrm{d}t,$$

where the inviscid and viscous fluxes are included in the integration of a single distribution function. The extension of the current scheme to the Rayleigh–Bénard simulation was given in [25].

3. Numerical experiments

The above gas-kinetic BGK scheme and the LBM are tested in the 2D cavity flow case. There is complicated wave structure involved in this case and highly accurate solutions have been obtained by Ghia et al. [5], and lately by Botella and Peyret [3]. The Ghia's results are based on finite difference scheme for the stream-vorticity formulation. Recently, Botella and Peyret use Chebyshev collocation method and improved solutions are obtained using a subtraction method around the corners (singularities) for the case of Reynolds number 1000. More importantly, the benchmark pressure data along the centerlines is presented in [3]. For the cavity flow, due to its simple geometry several higher-order compact schemes were proposed, which produced highly accurate results using less grid points, e.g. [12,19].

The computational mesh used for both LBM and gas-kinetic BGK schemes is 257×257 grid points. For the gas-kinetic BGK scheme, the time-step is determined by the CFL condition, i.e., $\Delta t = \eta \Delta x / (|\mathbf{u}|_{\max} + C)$, where C is the sound speed $C = \sqrt{1/2\lambda}$. In all calculations, a time-step with CFL number η equal to 0.5 is used. For very low Reynolds number flow simulation, such as $Re = 10$, another criteria for the time-step, i.e., $(\Delta x)^2/\nu$, has to be imposed. The Mach number used for the gas-kinetic BGK scheme is 0.15. In terms of boundary condition, a ghost cell inside boundary is created with the density ρ_{-1} and momentum $\rho_{-1}\mathbf{u}_{-1}$. For the non-slip boundary condition, we have

$$\rho_{-1} = \rho_1 \quad \text{and} \quad \rho_{-1}\mathbf{u}_{-1} = -\rho_1 \mathbf{u}_1,$$

where 1 refers to the first cell inside the domain. In the cavity case, the up-wall is moving with velocity $\mathbf{u}_0$, therefore, the flow variables in the ghost cell there is set to be $\rho_{-1} = \rho_1$ and $\rho_{-1}\mathbf{u}_{-1} = 2\rho_1\mathbf{u}_0 - \rho_1\mathbf{u}_1$. After setting up the values at the ghost cells, the boundary is treated as other cells inside the domain and the fluxes across the boundary are calculated by the method presented in the last section.

The boundary condition for the LBM simulations uses the bounce-back rule for non-equilibrium distribution which was outlined in [7]. This boundary condition is consistent with Grad's thirteen moment expansion theory for gas-kinetic theory. The velocity at the moving wall is fixed and the density is adjusted automatically according to the non-equilibrium bouncing rule. Special attention needs be applied to the boundary condition at the upper corners where singularity occurs. Treating the corners as parts of the top moving wall would underestimate the pressure difference between two corners; while treating the corners as parts of the stationary side walls would over-predict the pressure difference. A more realistic approach is compromising between these two restraints. In our LBM simulations, we implement this by assigning the incoming horizontal distribution function at the upper corners with the average of the outgoing horizontal distribution functions there.

Since the gas-kinetic BGK scheme and LBM are transient flow solvers, in order to get a steady state solution, the gas-kinetic BGK and LBM are run at least 500,000 time steps for each case. For the high Reynolds number case, more time steps are used. The simulation results, as well as the benchmark solutions, are presented in Figs. 3–5 for Reynolds numbers 1000, 5000, and 7500, respectively. In all cases, almost identical solutions are obtained from both the gas-kinetic BGK scheme and the LBM. With the

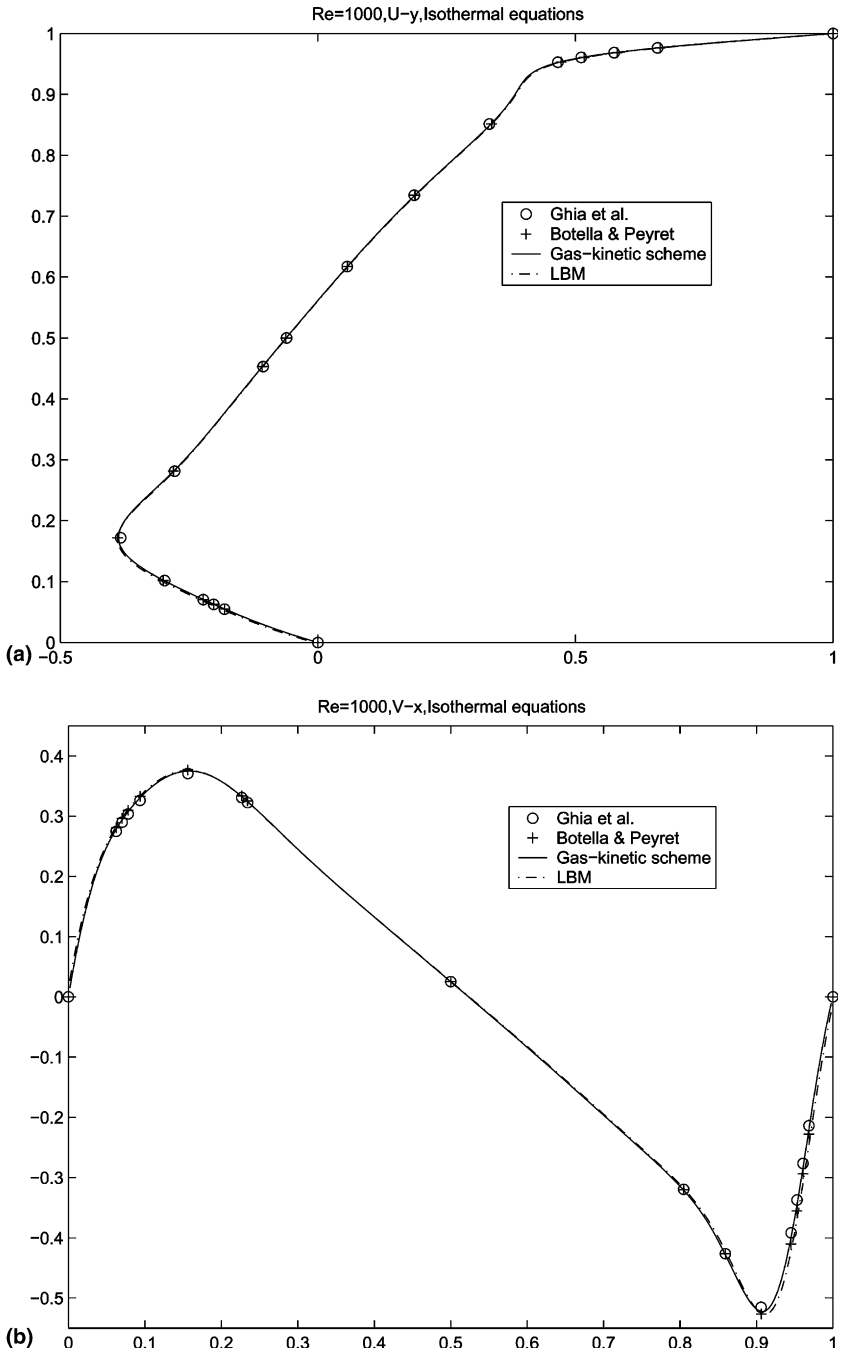

Fig. 3. Velocity and pressure distributions calculated by the LBM and gas-kinetic BGK scheme along the central lines at $Re = 1000$. The benchmark results are from Ghia et al. [5] and Botella and Peyret [3].

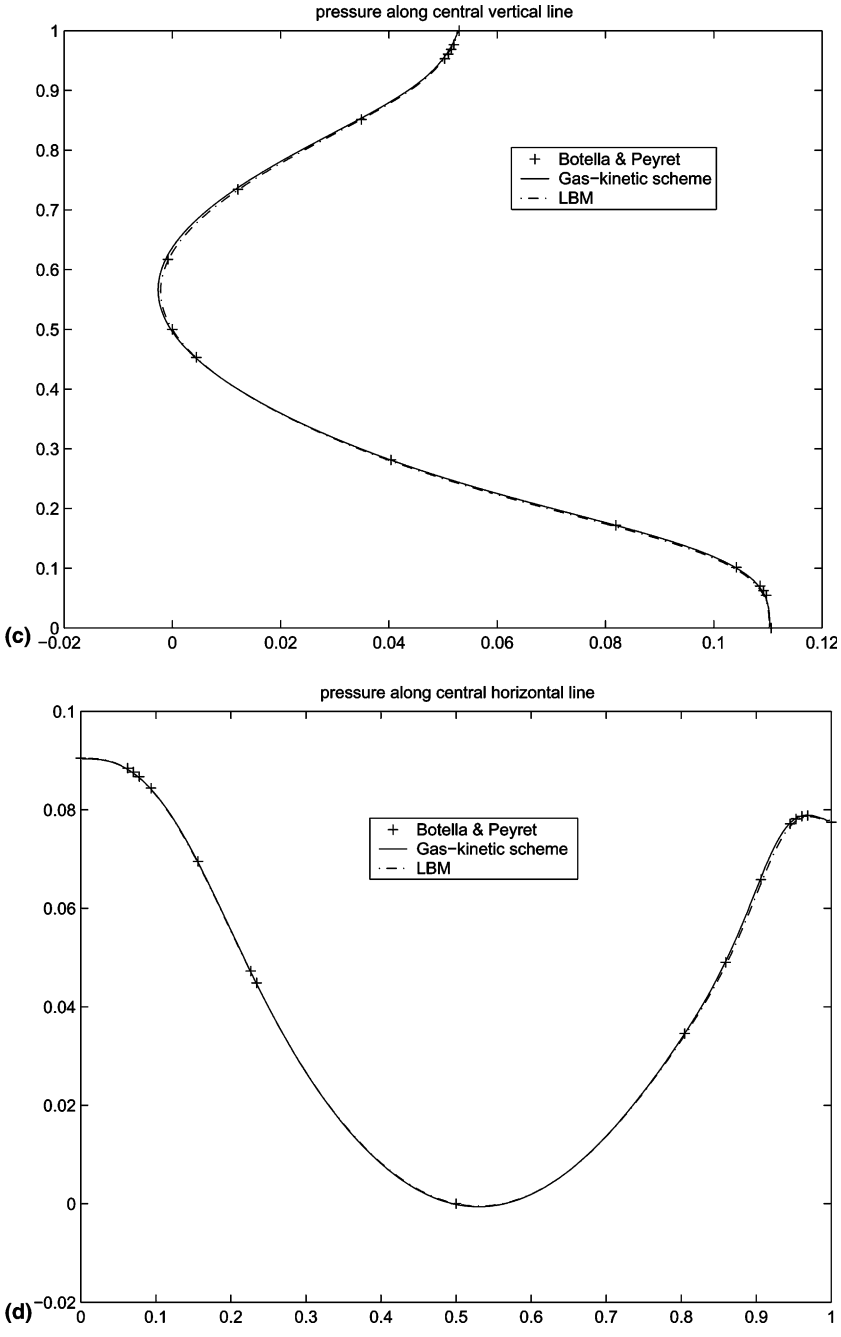

Fig. 3. (*continued*)

Reynolds number increased to 5000, the pressure distributions start to exhibit some oscillation, even though the velocity distributions are smooth and close to the Ghia et al.'s results. These oscillations will enhance more at even higher Reynolds number (data not shown), and bifurcations appear [17]. We suspect these oscillations are due to acoustic waves and plan to carry further studies on this subject in future.

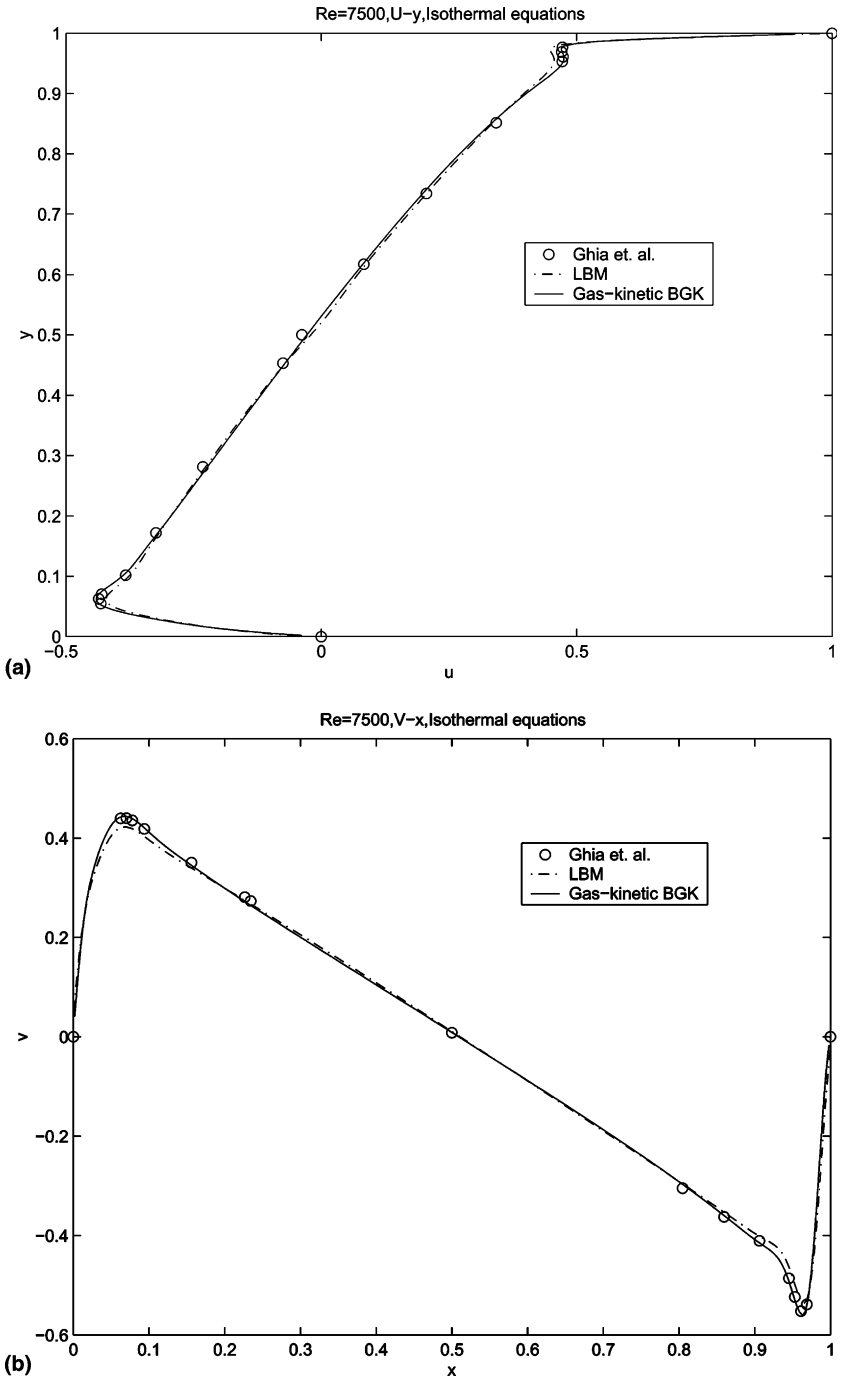

Fig. 4. Simulation results from the LBM and gas-kinetic BGK scheme at $Re = 5000$, where only Ghia et al. [5] benchmark results (velocity) are available.

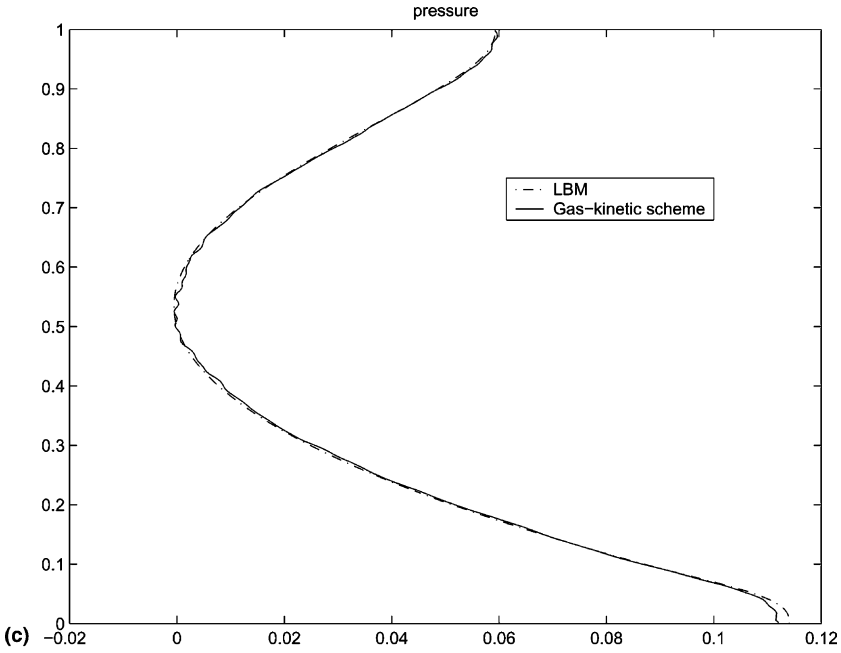

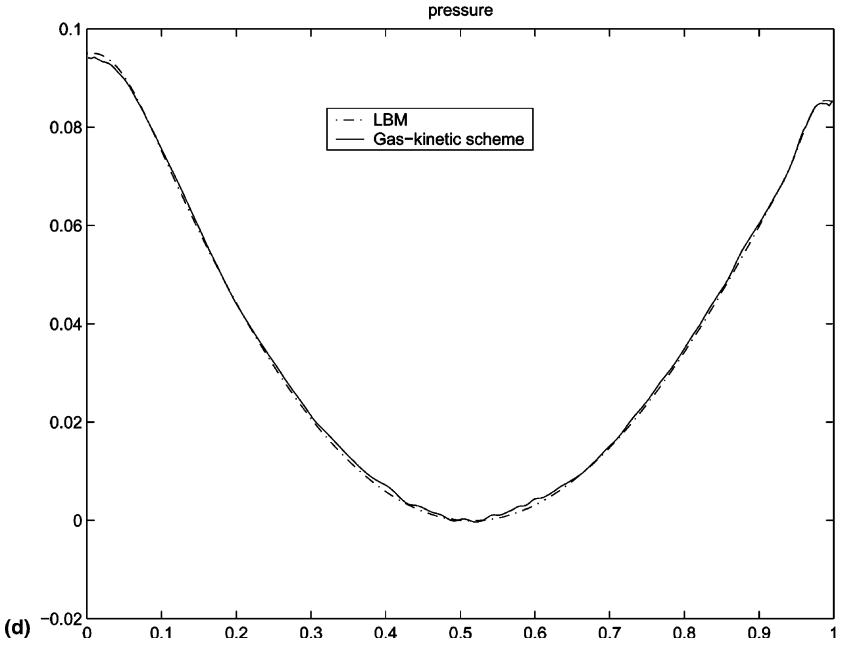

Fig. 4. (*continued*)

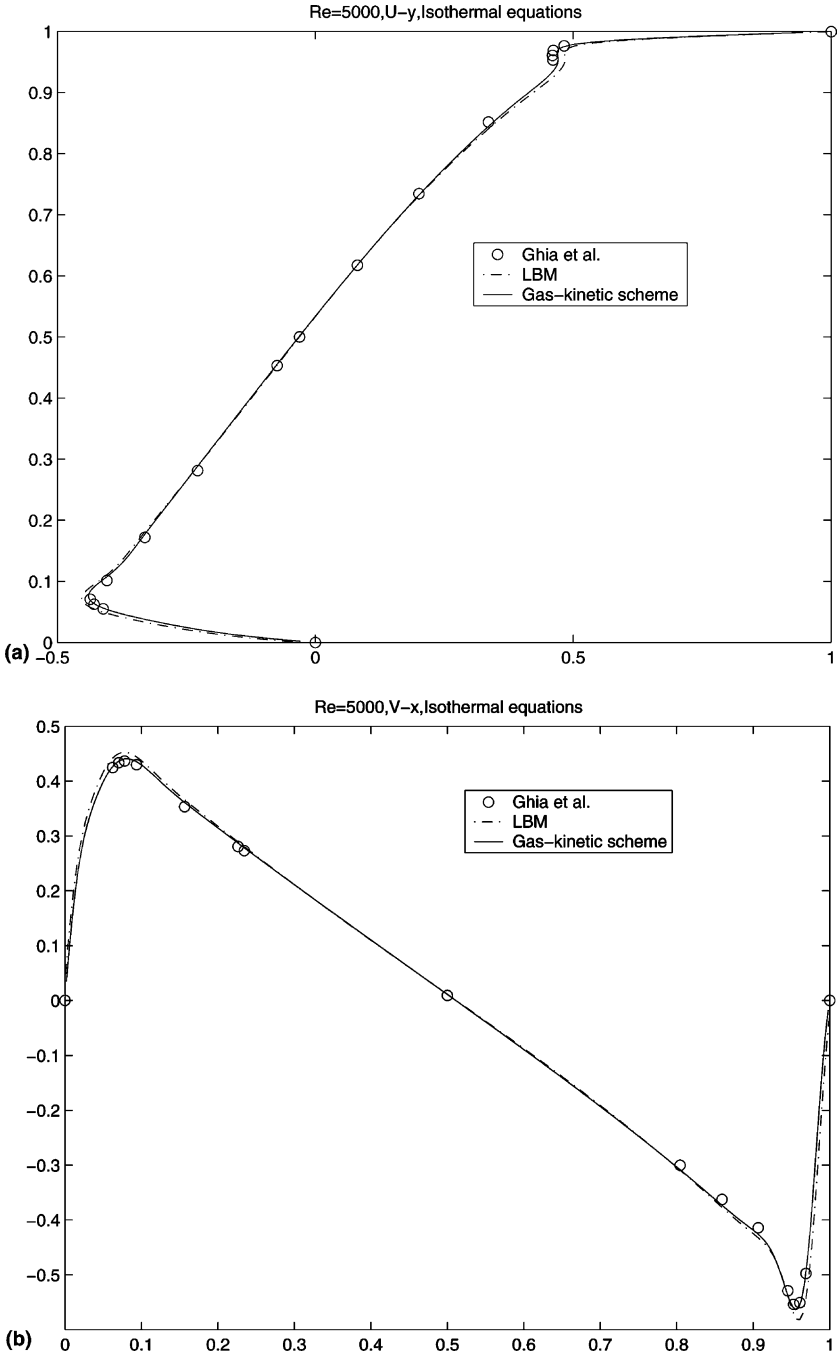

Fig. 5. Simulation results from the LBM and gas-kinetic BGK scheme at $Re = 7500$.

4. Conclusion

In this paper, for the first time two schemes based on the gas-kinetic Boltzmann equation are compared in the simulation of low speed, nearly incompressible flows. Due to the same intrinsic governing equation, both schemes are equivalent to solving the compressible isothermal Navier–Stokes equations. Comparable solutions are obtained from both schemes. In terms of boundary treatment, both schemes are easy to implement different kind of boundary conditions, such as isothermal, adiabatic, non-slip, etc. The numerical results in this paper demonstrate that a compressible code can be confidently used in the incompressible flow simulation for a velocity field, and the Mach number does not need to take a very small value. The understanding of the operator splitting and average models from the Boltzmann equation and their connection to the LBM and many other kinetic schemes need to be clarified in future.

Acknowledgements

We would like to thank Drs. L.S. Luo and C. Loh for helpful discussion. This work for K.X. was supported by the Research Grant Council of Hong Kong.

Appendix A. Interpolation of macroscopic flow variables at point 0 of Fig. 2

With the known cell averaged conservative quantities $w = (\rho, \rho\mathbf{u})^{\mathrm{T}}$ at cells 1, 2, 3, and 4, first we can use a third-order interpolation to get the pointwise values at point 0

$$w_0 = \frac{7}{12}(w_2 + w_3) - \frac{1}{12}(w_1 + w_4),$$

and the corresponding slope in x-direction becomes

$$\frac{\partial w}{\partial x} = \frac{5}{4}(w_3 - w_2)/\Delta x - \frac{1}{12}(w_4 - w_1)/\Delta x.$$

If w_0 is outside the range determined by w_2 and w_3, a second-order interpolation is used

$$w_0 = \frac{1}{2}(w_2 + w_3)$$

and

$$\frac{\partial w}{\partial x} = (w_3 - w_2)/\Delta x.$$

Similarly, the pointwise values at points 5 and 6, such as w_5 and w_6, can be obtained from the cell averaged values on their rows. Therefore, the y-derivative for w at point 0 is constructed as

$$\frac{\partial w}{\partial y} = \begin{cases} (w_5 - w_6)/2\Delta y & \text{if } (w_5 - w_0)\cdot(w_0 - w_6) \geqslant 0, \\ 0 & \text{if } (w_5 - w_0)\cdot(w_0 - w_6) < 0. \end{cases}$$

At the boundary of the cavity flow, only a second-order interpolation is used in the construction of w_0 and the corresponding gradients.

Appendix B. Determination of the coefficients of a Maxwellian expansion

In the gas-kinetic scheme, from the moments we need to evaluate the parameters in the expansion of gas distribution function. With a Maxwellian distribution function g

$$g = \rho\left(\frac{\lambda}{\pi}\right)\mathrm{e}^{-\lambda((\xi_x-u)^2+(\xi_y-v)^2)},$$

we have the following moments:

$$\int\int \begin{pmatrix} 1 \\ \xi_x \\ \xi_y \end{pmatrix} (a_1 + a_2\xi_x + a_3\xi_y) g \,\mathrm{d}\xi_x \,\mathrm{d}\xi_y = \begin{pmatrix} \tilde{b}_1 \\ \tilde{b}_2 \\ \tilde{b}_3 \end{pmatrix} \equiv \begin{pmatrix} \partial\rho/\partial x \\ \partial(\rho u)/\partial x \\ \partial(\rho v)/\partial x \end{pmatrix},$$

where both g and $(\tilde{b}_1, \tilde{b}_2, \tilde{b}_3)$ are known. The above equation can be rewritten as

$$\begin{pmatrix} b_1 \\ b_2 \\ b_3 \end{pmatrix} = \boldsymbol{M}\begin{pmatrix} a_1 \\ a_2 \\ a_3 \end{pmatrix}, \tag{B.1}$$

where $\mathbf{b} = \tilde{\mathbf{b}}/\rho$ and the matrix $\boldsymbol{M}$ has the form

$$\boldsymbol{M} = \begin{pmatrix} 1 & u & v \\ u & u^2 + 1/2\lambda & uv \\ v & uv & v^2 + 1/2\lambda \end{pmatrix}.$$

Defining

$$r_2 = b_3 - vb_1,$$

$$r_1 = b_2 - ub_1$$

the solutions of Eq. (B.1) are

$$a_3 = 2\lambda r_2,$$

$$a_2 = 2\lambda r_1,$$

and

$$a_1 = b_1 - ua_2 - va_3.$$

The above solution can also be used to evaluate both b and A, because the matrix $\boldsymbol{M}$ is identical in all these cases.

References

[1] F.J. Alexander, H. Chen, S. Chen, G.D. Doolen, Lattice Boltzmann model for compressible fluids, Phys. Rev. A 46 (1992) 1967.
[2] G.A. Bird, Molecular Gas Dynamics and the Direct Simulation of Gas Flows, Oxford University Press, Oxford, 1994.
[3] O. Botella, R. Peyret, Benchmark spectral results on the lid-driven cavity flow, Computers Fluids 27 (1998) 421–433.
[4] S.Y. Chen, G.D. Doolen, Lattice Boltzmann method for fluid flows, Annu. Rev. Fluid Mech. 30 (1998) 329–364.
[5] U. Ghia, K.N. Ghia, C.T. Shin, High-Resolutions for incompressible flow using the Navier–Stokes equations and a multigrid method, J. Comput. Phys. 48 (1982) 387–411.

[6] X.Y. He, L.S. Luo, Theory of the lattice Boltzmann method: from the Boltzmann equation of the lattice Boltzmann equation, Phys. Rev. E 56 (6) (1997) 6811–6817.
[7] X.Y. He, S.Y. Chen, G.D. Doolen, A novel thermal model for the lattice Boltzmann method in incompressible limit, J. Comput. Phys. 146 (1998) 282–300.
[8] S. Hou, Q. Zou, S. Chen, G. Doolen, A. Cogley, Simulation of cavity flow by the lattice Boltzmann method, J. Comput. Phys. 118 (1995) 329–347.
[9] J. Huang, F. Xu, M. Vallieres, D.H. Feng, Y.H. Qian, B. Fryxell, M.R. Strayer, A thermal LBGK model for large density and temperature differences, Int. J. Modern Phys. C 8 (1997) 827.
[10] M. Junk, A. Klar, Discretization for the incompressible Navier–Stokes equations on the lattice Boltzmann method, SIAM J. Scientific Comput. 22 (2000) 1–19.
[11] Y.G. Lai, C.L. Lin, J. Huang, Accuracy and efficiency study of lattice Boltzmann method for steady-state flow simulations, Numer. Heat Transfer B 39 (2001) 21–43.
[12] M. Li, B. Fornberg, T. Tang, A compact fourth order finite difference scheme for the steady incompressible Navier–Stokes equations, Int. J. Numer. Methods Fluids 20 (1995) 1137–1151.
[13] R.J. Mason, A multi-speed compressible lattice Boltzmann model, J. Statist. Phys. 107 (2002) 385.
[14] B.T. Nadiga, An Euler solver based on locally adaptive discrete velocities, J. Statist. Phys. 81 (1995) 129.
[15] T. Ohwada, Higher order approximation methods for the Boltzmann equation, J. Comput. Phys. 139 (1998) 1–14.
[16] T. Ohwada, On the construction of kinetic schemes, J. Comput. Phys. 177 (2002) 156–175.
[17] M. Poliashenko, C.K. Aidun, A direct method for computation of simple bifurcations, J. Comput. Phys. 121 (1995) 246–260.
[18] D.I. Pullin, Direct simulation methods for compressible inviscid ideal gas flow, J. Comput. Phys. 34 (1980) 231.
[19] W.F. Spotz, G.F. Carey, High-order compact scheme for the steady stream-function vorticity equations, Int. J. Numer. Methods Eng. 38 (1995) 3497–3512.
[20] M.D. Su, K. Xu, M.S. Ghidaoui, Low-speed flow simulation by the gas-kinetic scheme, J. Comput. Phys. 150 (1999) 17–39.
[21] S. Succi, The Lattice Boltzmann Equation for Fluid Dynamics and Beyond, Clarendon Press, Oxford, 2001.
[22] C.H. Sun, Adaptive lattice Boltzmann model for compressible flows: viscous and conductive properties, Phys. Rev. E 61 (4) (2000) 2645.
[23] D.A. Wolf-Gladrow, Lattice-Gas Cellular Automata and Lattice Boltzmann Models, Springer, Berlin, 2000.
[24] K. Xu, A gas-kinetic BGK scheme for the Navier–Stokes equations and its connection with artificial dissipation and Godunov method, J. Comput. Phys. 171 (2001) 289–335.
[25] K. Xu, S.H. Lui, Rayleigh–Bénard simulation using the gas-kinetic Bhatnagar–Gross–Krook scheme in the incompressible limit, Phys. Rev. E 60 (1999) 464.
[26] K. Xu, L.S. Luo, Connection between Lattice Boltzmann equation and beam scheme, Int. J. Modern Phys. C 9 (8) (1998) 1177–1187.